Reconstruction of nanoparticle size distribution in laser-shocked matter from SAXS via neural networks

Z. He[1,2,3], J. Lütgert[1,2], M. G. Stevenson[2], B. Heuser[1,2], D. Ranjan[1,2], C. Qu[2], and D. Kraus[1,2]

[1] *Helmholtz-Zentrum Dresden-Rossendorf, Bautzner Landstrasse 400, 01328 Dresden, Germany*

[2] *Institut für Physik, Universität Rostock, 18051 Rostock, Germany*

[3] *Shanghai Institute of Laser Plasma, 201800 Shanghai, China*

Abstract

Small angle X-ray scattering (SAXS) has been widely used as a microstructure characterization technology. In this work, a fully connected dense forward network is applied to inverse the mean particle size and particle distribution from SAXS data of samples dynamically compressed with high-power lasers and probed with X-ray free electron lasers. The trained network allows automatic acquisition of microstructure information, performing well in predictions on single-species nanoparticles on theoretical model and *in situ* experimental data. We evaluate our network by comparing it with other methods, revealing its reliability and efficiency in dynamic experiments, which is of great value for *in situ* characterization of materials under high-power

Correspondence to: Email: hezy1213@foxmail.com; Correspondence to: Email: dominik.kraus@uni-rostock.de

This peer-reviewed article has been accepted for publication but not yet copyedited or typeset, and so may be subject to change during the production process. The article is considered published and may be cited using its DOI.

10.1017/hpl.2024.27

laser driven dynamic compression.

Keywords: small angle X-ray scattering; machine learning; *in situ* X-ray diagnostics; shock compressed matter

1. Introduction

The dynamic mechanical properties of materials are strongly dependent on the temporal evolution of material structures at the micro mesoscale, and has important applications in extreme scenarios such as celestial evolution and inertial confinement fusion[1–3]. The average grain size and grain distribution are the key microstructure characteristics that affect the physical and chemical properties[4–6], representing the fundamental qualities of polycrystalline materials, therefore are of vital importance in predicting material responses, evaluating the kinetic phase transformation process, and having a insight into the physical connotations.

As a microstructure characterization technology, small angle X-ray scattering (SAXS) is of significant value in high-pressure material science[7–10] and high-power laser experiments[11,12]. In a typical scattering experiment, the X-ray impacts the sample at a small angle and scatters. The intensity of the scattered wave is measured and recorded by the detector and presented as a scattering pattern. For example, in the dynamic compressed experiment of polymer dissociation, nano crystalline solid particles can be formed and then consolidated into larger particles[13,14]. In the process of nucleation and subsequent phase transformation in such materials[15], the average particle size, grain distribution, particle shape, spacing, particle content and other microstructure characteristics will all affect the morphology and intensity of the scattering spectrum.

The inversion of nanoparticles due to phase transition in extreme conditions is a major

https://doi.org/10.1017/hpl.2024.27 Published online by Cambridge University Press

challenge. Extracting particle size distribution from the scattering pattern is a typical ill-posed problem. Algorithms such as maximum entropy, renormalization, regularization, non-negative least squares method and other methods have been widely used to extract the particle size distribution from the scattering data and extensively implemented in softwares such as Irena, IsGISAXS and McSAS[16–20]. These algorithms are mainly searching for optimization parameters that satisfy the condition of χ^2=constant, where χ^2 describes the degree of correlation of the fitting. Among them, McSAS adopts the Monte Carlo method, which uses rejection sampling to optimize by replacing model contributions in the dataset. At the end of the optimization process, the fitting parameter values contributed by each model in the dataset determine the final size distribution. During the SAXS analysis process and the microstructure inversion, it is usually necessary to establish a sample model first, run simulations of the scattering process and compare them with the experimentally observed pattern, and then repeat the process numerous times as well as adjust several parameters until this model is closest to the experimental result. Running simulations for each optimization step is time-consuming and requires considerable computing power[21].

With the emergence of fourth generation X-ray free electron lasers, it is possible to quickly image and obtain *in situ* response of materials, e.g., in dynamic shock-compression environments[22]. Large quantities of data, with laser shock drivers reaching repetition rates of up to 10 Hz[23], also pose a demand for rapid inversion of SAXS. In recent years, with the continuous advent of machine learning, it is possible to quickly retrieve scattering images and conduct on-site analysis. In view of the strong mapping ability of artificial neural networks (ANN), it can be well applied to *in situ* classification and quantification of scattering images including grazing-incidence small angle scattering (GISAS)[24], coherent diffraction imaging (CDI)[25], microstructural

https://doi.org/10.1017/hpl.2024.27 Published online by Cambridge University Press

characterization in 3D samples[6], etc. The ability of ANN to quickly and accurately identify the main characteristics is very important for the rapid characterization of crystal grain distribution, thus having a practical significance for the research in microstructure and phase transformation of dynamically compressed materials.

In this work, we apply a fully connected dense feedforward network according to the principle of SAXS to extract the mean grain size and grain distribution of nanocrystals from *in situ* SAXS images in experiments, allowing automatic acquisition of microstructure information and avoiding the traditional tedious manual fitting. Using the trained network, the particle distributions obtained from simulation data are verified to be in good agreement with the theory. Taking a typical nanoparticle transformation experiment as an example[22], we use the network to retrieve the average grain size as well as the grain distribution, and compare it with other methods to ensure that the neural network prediction is meaningful and applicable for SAXS. This network is also suitable for the case of spherical voids in porous materials. And the beneficial modifications based on our network is applicable to the arbitrary size inversion of other shapes with density contrast from SAXS, which is of great value for the on-site characterization of materials under dynamic compression.

2. Training neural network

According to the principle of SAXS, we can establish a fully connected feedforward network corresponds exactly to our physical issures. The data set with various particle distributions as well as their volume fraction (representing particle concentration) are used as the labels of the network, while the corresponding scattering intensities are used as the input data set. For the predicted

https://doi.org/10.1017/hpl.2024.27 Published online by Cambridge University Press

particle distributions from the neural network, the loss function of the training and validation data can be calculated and the network parameters are adjusted to minimize the loss. The process can then be repeated for several epochs until the acceptable loss value is reached.

2.1. Data generation

The data set for the neural network is generated on the basis of the classical SAXS theory. The expected scattering intensity I_{abs} in absolute units can be defined using [26]

$$I_{abs}(q) = \varphi(1-\varphi)\cdot\left(\Delta\rho_s\right)^2 \cdot V \cdot |F(q)|^2 \cdot S(q), \tag{1}$$

where q is the wavenumber, φ is the volume fraction of the nanoparticles, 1-φ is the volume fraction of the solution, V is the volume of a single nanoparticle, $\Delta\rho_{\text{sl}}$ is the total scattering length density contrast between solids and solutions, $F(q)$ and $S(q)$ represent the form factor and structure factor respectively. When assuming spherical nanoparticles in one case, the form factor $F(q)$ can be expressed as

$$\begin{aligned} F(q) &= \int_0^R \int_0^{2\pi} \int_0^{\pi} e^{jqr\cos\theta} r^2 \sin\theta d\theta d\varphi dr \\ &= \frac{4}{3}\pi R^3 \cdot 3\frac{\sin(qR) - qR\cos(qR)}{(qR)^3}, \end{aligned} \tag{2}$$

where R is the effective radius of the scatter. By introducing the repellent potential $U(r)$ of hard-sphere in Percus-Yevick closure[27–30], the structure factor can be described as

$$S(q) = 1 + \rho_{\text{part}} \int g(r)\cdot e^{-iqr} dV. \tag{3}$$

We created a dataset of scattering intensity generated by hard-spheres with an effective particle size range of 1-9 nm and a volume fraction range of 0.1-0.5, that corresponds exactly to our physical issues[13,15,22]. For example, we estimated the size of the generated nanoparticles from

https://doi.org/10.1017/hpl.2024.27 Published online by Cambridge University Press

shock compressed polymer samples via other diagnostics (such as X-ray diffraction) to be several nanometers, with a volume fraction between 10-50 %. Considering the possible distribution range of actual grain size in these experiments, we chose particle size distribution between 0.9-9.9 nm as the target labels, represented by 100 equally discrete probability values. When creating a random particle size distribution, we selected the composition of three shulz distributions with random effective radii as the total probability for different particle sizes. To assess the robustness of the network, we artificially added 0-3% random error as noise to the theoretical SAXS intensity data. This is based on the fact that the error of SAXS lineouts obtained on high energy X-ray light source is mainly related to the instrument and light source quality, which causes an intensity error of less than 2%[22]. ANN can generalize well to any particle size distribution by training on this simple data. In addition, the q range that can be detected by SAXS detector from beamline experiments is about 0.4-1.05 nm^{-1}. Correspondingly, we selected the same q range of scattering intensity in our ANN dataset, and took 1000 equally discrete intensity values within this range as well as the volume fractions (which can be estimated by comparing static experiments with dynamic experiments) as the input set (see Fig. 1 for the input and output parameters). The detailed parameter information in the dataset is shown in Table 1. We set 80% of the data in the dataset as the validation set and the remaining 20% as the testing set.

https://doi.org/10.1017/hpl.2024.27 Published online by Cambridge University Press

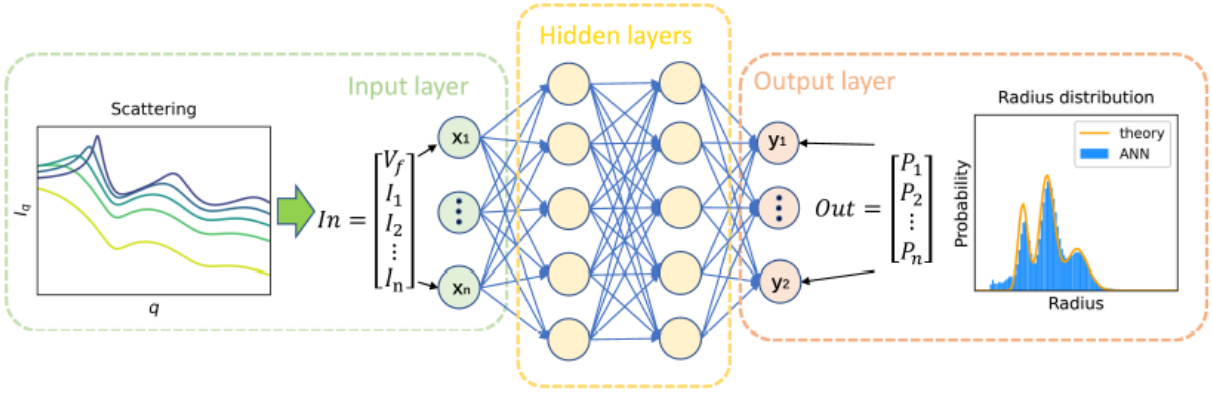

Figure 1. Schematics of traning process.

https://doi.org/10.1017/hpl.2024.27 Published online by Cambridge University Press

Table 1. Parameter ranges during data generation.

Parameter	Min value	Max value	Units
q	0.4	1.05	nm^{-1}
effective radius	1.0	9.0	nm
particle distribution	0.9	9.9	nm
volume fraction	10.0	50.0	%

In order to prevent the slow convergence of features during optimization[31], it is necessary to preprocess and normalize the data, which is an important step of neural network training. The entire data set was scaled after creating the train-validation databases so that all the input and target features were in the range [0, 1] according to

$$z_i' = \frac{z_i - \min(z)}{\max(z) - \min(z)}, \tag{4}$$

where z represents the data set of a certain feature, z_i represents a sample of z, and max(z) and min(z) are the maximum and minimum values of z, respectively. The scaling is undone afterward.

2.2. Compilation and training of the ANN

The compilation of the neural network and the training were performed using the Keras package running the Tensorflow backend[32].

We established a fully connected dense feedforward network according to our physical case with a rectified linear unit (ReLU)[33] as the nonlinear activation function. The input layer

https://doi.org/10.1017/hpl.2024.27 Published online by Cambridge University Press

includes 1000 discrete intensity values as well as one volume fraction value while the output layer contains 100 discrete probability values representing size distribution. The middle three hidden layers have 128, 64, and 32 neurons, respectively. We chose the mean absolute error (MAE) as the loss function in the training and testing process (see Eq. 5). The backpropagation[34] and the stochastic gradient descent optimization algorithm[35] were used to adjust the weights and biases iteratively until the loss function was minimized. In each iteration process, the network calculated the gradient of the batch loss relative to the weight and then updated the weight accordingly.

$$\mathrm{MAE}(X,h)=\frac{1}{m}\sum_{i=1}^{m}\left|h\left(x_i\right)-y_i\right|. \tag{5}$$

The ANN was trained along with adjusting the memorization capacity (the number of hidden layers or neurons) to find the optimal network structure avoiding underfit and overfit. In each training process, 4680 datasets with more than 4 million trainable parameters have been trained.

Figure 2 shows the training and validation loss or accuracy as a function of epoch. The validation loss is very close to the training loss, indicating that although the model is complex, it does not over fit the training data, and has good generalization ability in the verification dataset.

3. Evaluation of the trained network

Based on the trained neural network, the grain distribution can be quickly and reliably retrieved from scattering data. Therefore, the property of the trained network should be evaluated by measuring its performance in a large number of theoretical data.

https://doi.org/10.1017/hpl.2024.27 Published online by Cambridge University Press

3.1. Apply ANN to the theoretical models

Figure 3 depicts the predictions of the trained ANN on several theoretical data. After inputting the theoretical SAXS intensity lineout data with 0-3% noise to the trained ANN, the network can directly give the particle distribution, as shown in the blue histogram in the right column of Fig. 3. Aiming at arbitrary particle distribution with various patterns, our predicted particle distribution and the effective radius are in good agreement with the theoretical ones. Conversely, the corresponding SAXS lineout can also be calculated from the predicted distribution, as shown in the left column of Fig. 3, which is almost consistent with the original theoretical SAXS lineout in the majority of cases, implying a high reliability in the prediction of arbitrary particle distributions from theoretical data with noise.

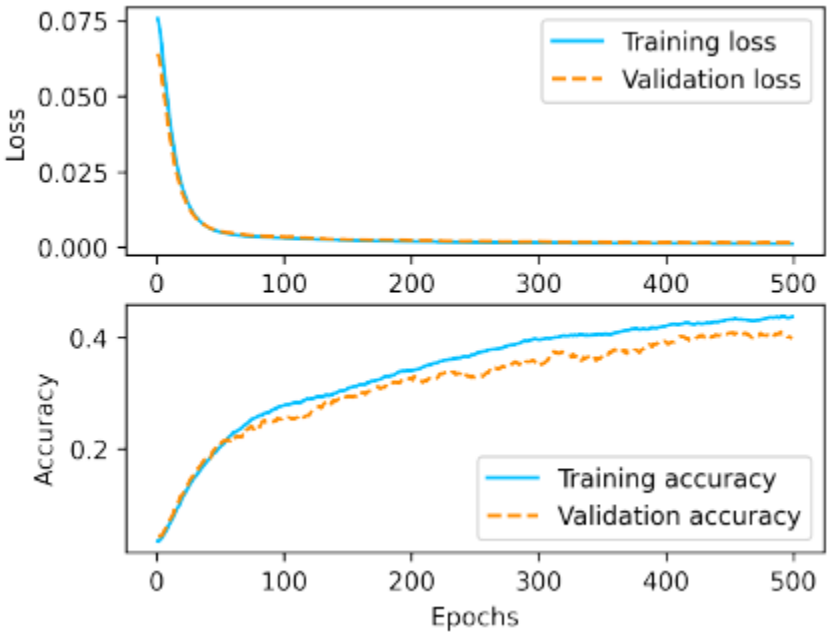

Figure 2. Training and validation loss as well as accuracy of the neural network which contains 3 middle hidden layers with 128, 64, 32 neurons respectively.

https://doi.org/10.1017/hpl.2024.27 Published online by Cambridge University Press

However, for simple distributions with small particle radii, the difficulty of fitting increases due to the tiny variation of scattering intensity in the range of $0.4\text{-}1.05\,\mathrm{nm}^{-1}$, as shown in the first panel in the right column of Fig. 3. The more complex the intensity curve and the larger the particle radius, the higher the fitting accuracy.

3.2. Apply ANN to the experiments

In order to evaluate the performance of ANN on the experimental data, we assess ANN with the real-time *in situ* SAXS experimental data measured in dynamic experiments. Five SAXS intensity data of shock compressed $100\ \mu\mathrm{m}$ PET[36] at various probing times under ： 100 GPa have been obtained on the Linac Coherent Light Source (LCLS) laser facility. The details of the experiment can be referenced in the previous work[22]. The *in situ* SAXS lineout data was used as input of the network, the particle distribution can then be predicted by the trained ANN. As shown in Fig.4, the predicted distributions at various probing times are compared with those obtained from an analytical method (applying the non-negative least squares method)[26] and the Monte Carlo method[19,20]. The left panel reveals the particle radius distribution obtained by the three methods, while the right panel exhibits the corresponding fitting lineouts. Interestingly, the three methods consistently point out that the mean particle size gradually increases with time in the shock compressed PET. It can be seen that the mean size predicted by ANN is relatively close to that of the Monte Carlo, and both of these two methods can obtain arbitrary size distribution and find a more discrete distribution at the last two probing times. As an analytical model, a Schultz distribution[37,38] is assumed with the polydispersity $p = \sigma / R \approx 0.1$, resulting in systematically lager effective radius at latter times than that of the another two methods. In fact, due to the

https://doi.org/10.1017/hpl.2024.27 Published online by Cambridge University Press

complexity of the dynamic compression process, the nanoparticles generated from the sample are usually too discrete and too arbitrary to be simply represented by a certain distribution. Therefore, the acquisition of arbitrary distribution from raw SAXS data will better reflect the actual situation, as predicted by ANN and Monte Carlo. Of course, in the actual experimental process, one still need to azimuthally integrate the original two-dimensional scattering pattern as well as subtract the backgrounds, which requires batch processing on written codes and usually takes a few minutes to complete. Afterwards, among the three methods, ANN can invert the particle distribution from the scattering data with a few milliseconds of compute time on a standard laptop, while Monte Carlo takes 10-30 minutes and the analytical method requires even more time per shot because if often requires manual input to assert good convergence, and therefore poses challenges when scaled to high-repetition-rate experiments or online analysis. Comparatively, in the experimental process of compact beam time from raw image to size distribution, ANN is very suitable for *in situ* data analysis, which is of great significance for the promotion of physical experiments and timely parameter adjustment. In further research, the process parameters of the Monte Carlo method, such as local volume fraction and scattering length density, can serve as intermediate inputs for ANN to fine tune the network. This kind of physics-informed neural network (PINN) is very promisingly beneficial for improving the accuracy of size distribution inversion from experimental data.

Other aspects of actual experiments, such as the bandwidth and the high harmonics of the probe light spectrum, can also affect the size distribution inversion from SAXS[39]. For the shock compression phase transition described above, the accuracy of the experiment itself is not so high that the influence of the spectrum bandwidth and high harmonics can be ignored. Of course, in some more precise SAXS inversion problems, the influence of spectrum cannot be ignored. In these cases, the ANN can be constructed through the following methods: directly input the

https://doi.org/10.1017/hpl.2024.27 Published online by Cambridge University Press

scattering spectrum and particle size distribution obtained from the specified spectrum into the ANN for training; Or add parameters representing the spectral features to the ANN for training.

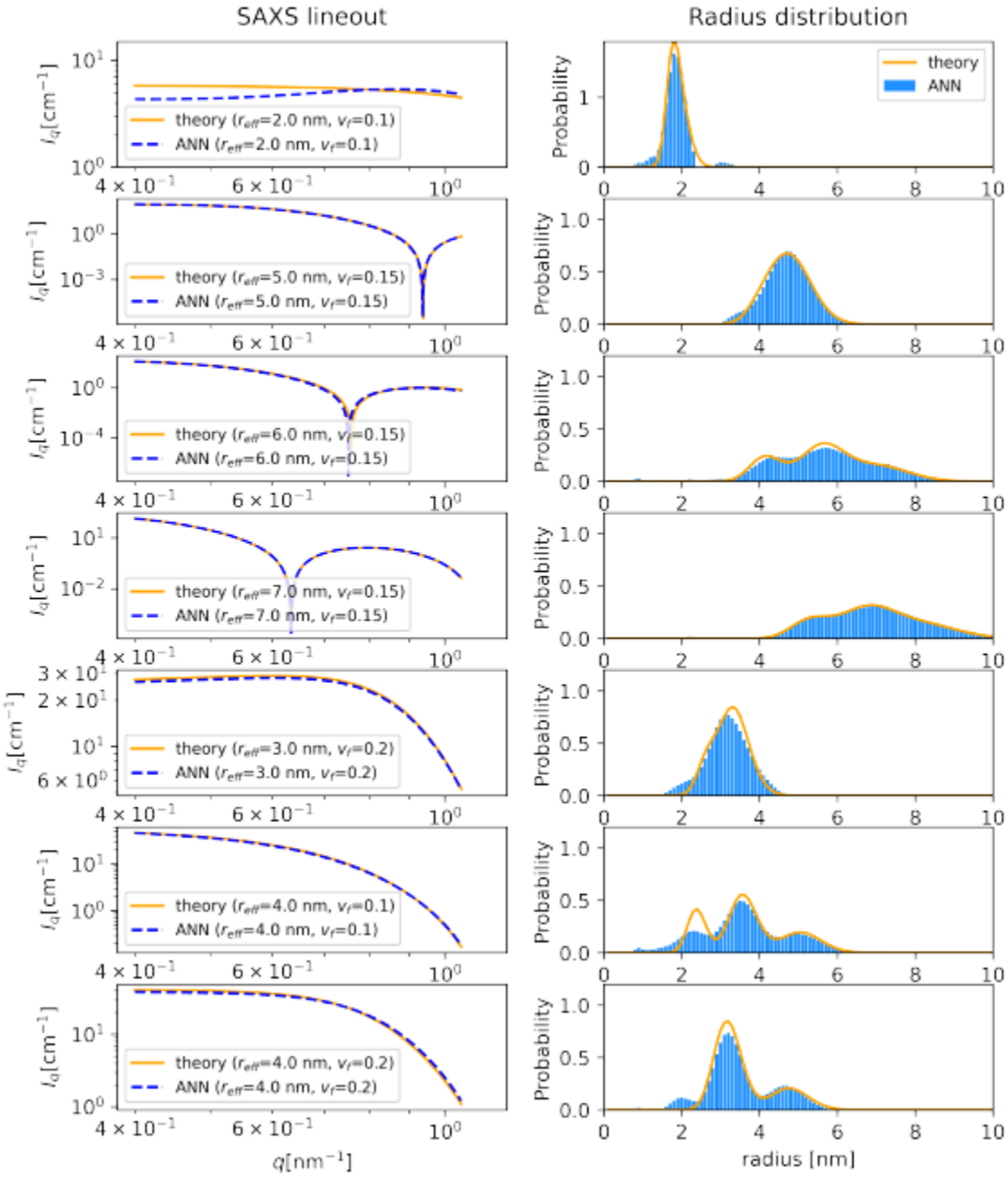

Figure 3. Apply ANN to the theoritical models. Seven arbitrary particle distributions predicted by ANN (right panel) and their corresponding fitting curves (left panel) compared with the initial

https://doi.org/10.1017/hpl.2024.27 Published online by Cambridge University Press

theoretical models.

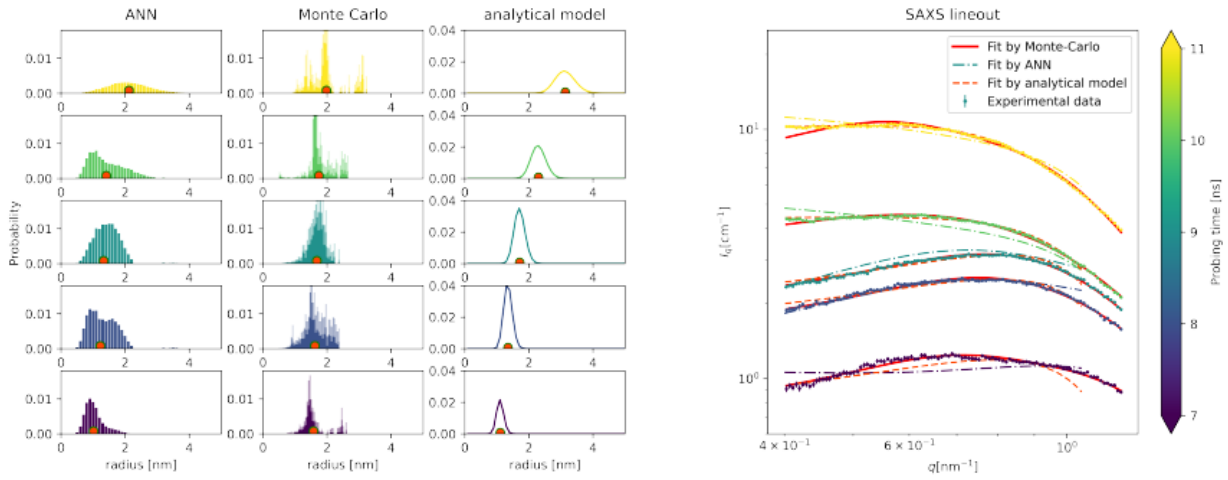

Figure 4. The nanoparticle distributions generated from shock compressed PET obtained by ANN, Monte Carlo and analytical model (left panel) and their corresponding SAXS fitting curve compared with the experimental data (right panel). The red dots indicate the resulting mean particle radius from the three methods. The color bar represents the various probing times.

4. CONCLUSIONS

To conclude, in view of the request for rapid analysis of generous SAXS data on large-scale laser facilities, in this work, we apply a dense forward network to inverse the mean grain size and particle distribution from SAXS data, allowing automatic acquisition of microstructure information without tedious manual fitting in traditional methods. Our trained network performs well in grain distribution prediction on experimental data with single-species particles. The predicted results have good consistency with the Monte Carlo method, which also inverses

https://doi.org/10.1017/hpl.2024.27 Published online by Cambridge University Press

arbitrary distribution, and is more efficient.

Since the scattering intensity comes from density contrast, theoretically, our trained network can also be applied to the case of void distribution with spherical shapes in porous materials, but its effectiveness still needs further experimental verification. In further work, two possible improvements can be considered if this network is to be applied to non-spherical particles or voids. One is that the network needs to be retrained for particles or voids of specific shapes, and the method of constructing and training the network can be consistent with this work. A more universal approach is to add additional factors representing the shape of particles to the input of the network on the basis of this method, and then retrain the network. In short, the powerful advantages of ANN can be utilized in the study of dynamic physical processes by adding scattering shape parameters, optimizing model structures, etc. In addition, improvements in the diagnosis of the experiment, such as increasing the scattering angle range and improving the signal-to-noise ratio, can also enhance the accuracy of the ANN model.

Acknowledgements Authors are grateful for the use of experimental data. This work was supported by the Helmholtz Association under VH-NG-1141 and ERC-RA-0041. Z.H. acknowledges the support from the National Science Foundation of China under Award No. 12304033 and the financial support from China Scholarship Council.

https://doi.org/10.1017/hpl.2024.27 Published online by Cambridge University Press

References

1. Choong-Shik Yoo. Chemistry under extreme conditions: Pressure evolution of chemical bonding and structure in dense solids. *Matter and Radiation at Extremes*, 5(1), 2020.
2. DH Kalantar, JF Belak, GW Collins, JD Colvin, HM Davies, JH Eggert, TC Germann, J Hawreliak, BL Holian, K Kadau, PS Lomdahl, MA Lorenzana, HE adn Meyers, K Rosolankova, MS Schneider, J Sheppard, JS Stolken, and JS Wark. Direct observation of the α-ε transition in shock-compressed iron via nanosecond x-ray diffraction. *Physical Review Letters*, 95(7):075502, 2005.
3. R Betti and OA Hurricane. Inertial-confinement fusion with lasers. *Nature Physics*, 12(5):435–448, 2016.
4. Offerman and E. S. Grain nucleation and growth during phase transformations. *Science*, 21(5595):179–179, 2002.
5. EJAM Arzt. Size effects in materials due to microstructural and dimensional constraints: a comparative review. *Acta materialia*, 46(16):5611–5626, 1998.
6. H. Chan, M. Cherukara, T. D. Loeffler, B. Narayanan, and Skrs Sankaranarayanan. Machine learning enabled autonomous microstructural characterization in 3d samples. *npj Computational Materials*, 6(1), 2020.
7. M Bagge-Hansen, S Bastea, JA Hammons, MH Nielsen, LM Lauderbach, RL Hodgin, P Pagoria, C May, S Aloni, A Jones, WL Shaw, EV Bukovsky, N Sinclair, RL Gustavsen, EB Watkins, BJ Jensen, DM Dattelbaum, MA Firestone, RC Huber, BC Ringstrand, JRI Lee, T van Buuren, LE Fried, and TM Willey. Detonation synthesis of carbon nano-onions via liquid carbon condensation. *Nature communications*, 10(1):3819, 2019.

https://doi.org/10.1017/hpl.2024.27 Published online by Cambridge University Press

8. Sandrine Humbert, O Lame, JM Chenal, C Rochas, and G Vigier. New insight on initiation of cavitation in semicrystalline polymers: in-situ saxs measurements. *Macromolecules*, 43(17):7212–7221, 2010.

9. Martin Bech, Simone Schleede, Guillaume Potdevin, Klaus Achterhold, Oliver Bunk, Torben H Jensen, Rod Loewen, Ron Ruth, and Franz Pfeiffer. Experimental validation of image contrast correlation between ultra-small-angle x-ray scattering and grating-based dark-field imaging using a laser-driven compact x-ray source: Experimentelle verifizierung des zusammenhangs zwischen röntgen-kleinwinkelstreuung und gitter-basierter röntgen-dunkelfeldbildgebung unter verwendung eines laser-getriebenen kompaktsynchrotrons. *Photonics & Lasers in Medicine*, 1(1):47–50, 2012.

10. YW Shi, YY Zhang, Sen Chen, and Sheng-Nian Luo. Small angle x-ray scattering of nanoporous membranes: Effects of geometry and concentration. *Materials Today Communications*, 34:105095, 2023.

11. Thomas Kluge, Melanie Rödel, Josefine Metzkes-Ng, Alexander Pelka, Alejandro Laso Garcia, Irene Prencipe, Martin Rehwald, Motoaki Nakatsutsumi, Emma E McBride, Tommy Schönherr, Marco Garten, Nicholas J Hartley, Malte Zacharias, Jörg Grenzer, Artur Erbe, Yordan M. Georgiev, Eric Galtier, Inhyuk Nam, Hae Ja Lee, Siegfried Glenzer, Michael Bussmann, Christian Gutt, Karl Zeil, Christian Rödel, Uwe Hübner, Ulrich Schramm, and Thomas E. Cowan. Observation of ultrafast solid-density plasma dynamics using femtosecond x-ray pulses from a free-electron laser. *Physical Review X*, 8(3):031068, 2018.

12. YJ Deng, YY Zhang, Zhurong Cao, S Chen, and SN Luo. Effects of beam divergence and polychromaticity on small angle x-ray scattering measurements with laser plasma sources.

https://doi.org/10.1017/hpl.2024.27 Published online by Cambridge University Press

AIP Advances, 12(2), 2022.

13. Dominik Kraus, J Vorberger, A Pak, NJ Hartley, LB Fletcher, S Frydrych, E Galtier, EJ Gamboa, DO Gericke, SH Glenzer, E Granados, MJ MacDonald, AJ MacKinnon, EE McBride, I Nam, P Neumayer, M Roth, AM Saunders, AK Schuster, P Sun, T van Driel, T Dppner, and RW Falcone. Formation of diamonds in laser-compressed hydrocarbons at planetary interior conditions. *Nature Astronomy*, 1(9):606–611, 2017.

14. D Kraus, NJ Hartley, S Frydrych, AK Schuster, K Rohatsch, M Rödel, TE Cowan, S Brown, E Cunningham, T Van Driel, L. B. Fletcher, E. Galtier, E. J. Gamboa, A. Laso Garcia, Dirk O. Gericke, E. Granados, P. A. Heimann, H. J. Lee, M. J. MacDonald, A. J. MacKinnon, E. E. McBride, I. Nam, P. Neumayer, A. Pak, A. Pelka, I. Prencipe, A. Ravasio, R. Redmer, A. M. Saunders, M. Schölmerich, M. Schörner, P. Sun, S. J. Turner, A. Zettl, R. W. Falcone, S. H. Glenzer, T. Döppner, and J. Vorberger. High-pressure chemistry of hydrocarbons relevant to planetary interiors and inertial confinement fusion. *Physics of Plasmas*, 25(5):056313, 2018.

15. AK Schuster, NJ Hartley, J Vorberger, T Döppner, T van Driel, RW Falcone, LB Fletcher, S Frydrych, E Galtier, EJ Gamboa, D. O. Gericke, S. H. Glenzer, E. Granados, M. J. MacDonald, A. J. MacKinnon, E. E. McBride, I. Nam, P. Neumayer, A. Pak, I. Prencipe, K. Voigt, A. M. Saunders, P. Sun, and D. Kraus. Measurement of diamond nucleation rates from hydrocarbons at conditions comparable to the interiors of icy giant planets. *Physical Review B*, 101(5):054301, 2020.

16. PR Jemian, JR Weertman, GG Long, and RD Spal. Characterization of 9cr-1movnb steel by anomalous small-angle x-ray scattering. *Acta metallurgica et materialia*, 39(11):2477–2487, 1991.

https://doi.org/10.1017/hpl.2024.27 Published online by Cambridge University Press

17. Jan Ilavsky and Peter R Jemian. Irena: tool suite for modeling and analysis of small-angle scattering. *Journal of Applied Crystallography*, 42(2):347–353, 2009.

18. Rémi Lazzari. Isgisaxs: a program for grazing-incidence small-angle x-ray scattering analysis of supported islands. *Journal of Applied Crystallography*, 35(4):406–421, 2002.

19. Brian R Pauw, Jan Skov Pedersen, Samuel Tardif, Masaki Takata, and Bo Brummersted Iversen. Improvements and considerations for size distribution retrieval from small-angle scattering data by monte carlo methods. *Journal of applied crystallography*, 46(2):365–371, 2013.

20. Ingo Breßler, Brian Richard Pauw, and Andreas F Thünemann. Mcsas: software for the retrieval of model parameter distributions from scattering patterns. *Journal of applied crystallography*, 48(3):962–969, 2015.

21. Lennart Gaus, Lothar Bischoff, Michael Bussmann, Eric Cunningham, Chandra B Curry, E Juncheng, Eric Galtier, Maxence Gauthier, Alejandro Laso García, Marco Garten, Siegfried Glenzer, Juncheng E, Jörg Grenzer, Christian Gutt, Nicholas J. Hartley, EmmaE. McBride, Josefine Metzkes-Ng, Lingen Huang, Uwe Hübner, Dominik Kraus, Bob Nagler, Motoaki Nakatsutsumi, Alexander Pelka, Irene Prencipe, Jan Nikl, Hae Ja Lee, Masato Ota, Lisa Randolph, Melanie Rödel, Youichi Sakawa, Hans-Peter Schlenvoigt, Michal Šmíd, Franziska Treffert, Katja Voigt, Ulrich Schramm, Karl Zeil, Thomas Kluge, and Thomas E. Cowan. Probing ultrafast laser plasma processes inside solids with resonant small-angle x-ray scattering. *Physical Review Research*, 3(4):043194, 2021.

22. Zhiyu He, Melanie Rödel, Julian Lütgert, Armin Bergermann, Mandy Bethkenhagen, Deniza Chekrygina, Thomas E Cowan, Adrien Descamps, Martin French, Eric Galtier, A.E. Gleason, G.D. Glenn, S.H. Glenzer, Y. Inubushi, N.J. Hartley, J.-A. Hernandez, B.

https://doi.org/10.1017/hpl.2024.27 Published online by Cambridge University Press

Heuser, O.S. Humphries, N. Kamimura, K. Katagiri, D. Khaghani, H.J. Lee, E.E. McBride, K. Miyanishi, B. Nagler, B. Ofori-Okai, N. Ozaki, S. Pandolfi, C. Qu, D. Ranjan, R. Redmer, C. Schoenwaelder, A.K. Schuster, M.G. Stevenson, K. Sueda, T. Togashi, T. Vinci, K. Voigt, J. Vorberger, M. Yabashi, T. Yabuuchi, L.M.V. Zinta, A. Ravasio, and D. Kraus. Diamond formation kinetics in shock-compressed c-h-o samples recorded by small-angle x-ray scattering and x-ray diffraction. *Science Advances*, 8(35):eabo0617, 2022.

23. U. Zastrau, M. McMahon, K. Appel, C. Baehtz, E. Brambrink, R. Briggs, T. Butcher, B. Cauble, B. Chen, H. Damke Damker, C. Deiter, J. Eggert, K. Falk, L. Fletcher, S.H. Glenzer, S. Göde, M. Harmand, A. Higginbotham, Z. Konôpková, D. Kraus, H.-P. Liermann, M. Nakatsutsumi, Pelka A., G. Priebe, R. Redmer, A. Schropp, R. Smith, P. Sperling, I. Thorpe, and S. Toleikis. Conceptual design report: Dynamic laser compression experiments at the hed instrument of european xfel. Technical Report XFEL.EU TR-2017-001, Dynamic Laser Compression at HED, Schenefeld, European X-Ray Free-Electron Laser Facility GmbH, 2017, Germany, 2017.

24. Walter Van Herck, Jonathan Fisher, and Marina Ganeva. Deep learning for x-ray or neutron scattering under grazing-incidence: extraction of distributions. *Materials Research Express*, 8(4):045015, 2021.

25. Mathew J Cherukara, Youssef SG Nashed, and Ross J Harder. Real-time coherent diffraction inversion using deep generative networks. *Scientific reports*, 8(1):1–8, 2018.

26. M Rödel. *Coherent X-ray Diffraction of Laser-driven Matter*. PhD thesis, Technische Universität Dresden, 2021.

27. MS Wertheim. Exact solution of the percus-yevick integral equation for hard spheres.

https://doi.org/10.1017/hpl.2024.27 Published online by Cambridge University Press

Physical Review Letters, 10(8):321, 1963.

28. Jerome K Percus and George J Yevick. Analysis of classical statistical mechanics by means of collective coordinates. *Physical Review*, 110(1):1, 1958.

29. David J Kinning and Edwin L Thomas. Hard-sphere interactions between spherical domains in diblock copolymers. *Macromolecules*, 17(9):1712–1718, 1984.

30. Jan Skov Pedersen. Determination of size distribution from small-angle scattering data for systems with effective hard-sphere interactions. *Journal of applied crystallography*, 27(4):595–608, 1994.

31. Y. Lecun, L. Bottou, G. B. Orr, and K. R. Muller. Efficient backprop. *neural networks tricks of the trade*, 1998.

32. F. Chollet. Keras: The python deep learning library. *Astrophysics Source Code Library*, 2018.

33. Abien Fred Agarap. Deep learning using rectified linear units (relu). *arXiv preprint arXiv:1803.08375*, 2018.

34. D. E. Rumelhart, G. E. Hinton, and R. J. Williams. Learning representations by back-propagating errors. *Nature*, 323, 1986.

35. Léon Bottou. Stochastic gradient descent tricks. In *Neural networks: Tricks of the trade*, pages 421–436. Springer, 2012.

36. J Lütgert, J Vorberger, NJ Hartley, K Voigt, M Rödel, AK Schuster, A Benuzzi-Mounaix, S Brown, TE Cowan, E Cunningham, T. Döppner, R. W. Falcone, L. B. Fletcher, E. Galtier, S. H. Glenzer, A. Laso Garcia, D. O. Gericke, P. A. Heimann, H. J. Lee, E. E. McBride, A. Pelka, I. Prencipe, A. M. Saunders, M. Schölmerich, M. Schörner, P. Sun, T. Vinci, A. Ravasio, and D. Kraus. Measuring the structure and equation of state of

https://doi.org/10.1017/hpl.2024.27 Published online by Cambridge University Press

polyethylene terephthalate at megabar pressures. *Scientific Reports*, 11(1):1–9, 2021.

37. Michael Kotlarchyk and Sow-Hsin Chen. Analysis of small angle neutron scattering spectra from polydisperse interacting colloids. *The Journal of chemical physics*, 79(5):2461–2469, 1983.

38. Jens Als-Nielsen and Des McMorrow. *Elements of modern X-ray physics*. John Wiley & Sons, 2011.

39. Sen Chen and S-N Luo. Small-angle scattering of polychromatic x-rays: effects of bandwidth, spectral shape and high harmonics. *Journal of Synchrotron Radiation*, 25(2):496–504, 2018.

https://doi.org/10.1017/hpl.2024.27 Published online by Cambridge University Press